Effects of detector blur and correlated noise on digital breast tomosynthesis reconstruction

Jiabei Zheng[*a,b], Jeffrey A. Fessler[a,b], Heang-Ping Chan[a]

[a]Department of Radiology
[b] Department of Electrical Engineering and Computer Science
University of Michigan, Ann Arbor, MI 48109

ABSTRACT

To improve digital breast tomosynthesis (DBT) image quality, we are developing model-based iterative reconstruction methods. We developed the SQS-DBCN algorithm, which incorporated detector blur into the system model and correlation into the noise model under some simplifying assumptions. In this paper, we further improved the regularization in the SQS-DBCN method by incorporating neighbors along the diagonal directions. To further understand the role of the different components in the system model of the SQS-DBCN method, we reconstructed DBT images without modeling either the detector blur or noise correlation for comparison. Visual comparison of the reconstructed images showed that regularizing with diagonal directions reduced artifacts and the noise level. The SQS-DBCN reconstructed images had better image quality than reconstructions without models for detector blur or correlated noise, as indicated by the contrast-to-noise ratios (CNR) of MCs and textural artifacts. These results indicated that regularized DBT reconstruction with detector blur and correlated noise modeling, even with simplifying assumptions, can improve DBT image quality compared to that without system modeling.

Keywords: Digital Breast Tomosynthesis, Model-based Iterative Reconstruction, Detector Blur, Correlated Noise

1. INTRODUCTION

Digital breast tomosynthesis (DBT) was developed to alleviate the problem of overlapping tissue in conventional two dimensional (2D) mammography. In DBT, commonly used reconstruction methods include filtered back-projection (FBP) [1-3] and iterative reconstruction (IR) methods [4-6]. To improve DBT image quality, we are developing model-based iterative reconstruction (MBIR) method based on models of the imaging system physics. Our preliminary implementation [7] incorporated detector blur into the system model and correlation into the noise model under some simplifying assumptions, and used a separable quadratic surrogate (SQS) algorithm for minimizing the cost function. We also replaced the traditional ray-tracing projector with the segmented separable footprint projector (SG projector) [8]. We referred to this reconstruction method as the SQS-DBCN algorithm. We have shown that SQS-DBCN improves DBT image quality, especially for microcalcification (MC) clusters that are one of the important signs of early breast cancer.

In the current study, we continue to refine the SQS-DBCN algorithm. We introduced regularization along the diagonal directions to reduce the textural artifacts in the reconstructed images. To investigate the effects of the detector blur model and the correlated noise model on DBT image quality, we reconstructed the images of phantoms and human subjects by removing one of the model components at a time and compared these images with those reconstructed with both components. The contrast-to-noise ratios (CNR) of MCs from the phantoms over a range of parameters and the visual quality of the human subject images under different reconstruction conditions were used to evaluate the effectiveness of the model components in the SQS-DBCN method.

[*] Correspondence: jiabei@umich.edu

Medical Imaging 2017: Physics of Medical Imaging, edited by Thomas G. Flohr, Joseph Y. Lo, Taly Gilat Schmidt, Proc. of SPIE Vol. 10132, 1013226 · © 2017 SPIE
CCC code: 1605-7422/17/$18 · doi: 10.1117/12.2255689

2. METHODS AND MATERIALS

2.1 Regularization with Eight Neighboring Pixels

In the SQS-DBCN method for DBT, we consider the following reconstruction problem:

$$\hat{\mathbf{f}}_{full} = \text{argmin}_{\mathbf{f}} \frac{1}{2} \sum_i \|\mathbf{y}_i - \mathbf{B}_i \mathbf{A}_i \mathbf{f}\|^2_{(\mathbf{B}_i \mathbf{K}_i^q \mathbf{B}_i' + \mathbf{K}_i^r)^{-1}} + R(\mathbf{f}), \tag{1}$$

where $\mathbf{f}$ is the image to reconstruct, $\mathbf{y}_i$ is the ith measured projection view (PV) after log transform, $\mathbf{A}_i$ is the projection matrix, $\mathbf{B}_i$ is the detector blur, $\mathbf{K}_i^q$ and $\mathbf{K}_i^r$ are diagonal covariance matrices of quantum noise and readout noise, respectively, and $R(\mathbf{f})$ is the regularization term. As a first approximation, we simplified the implementation of the SQS-DBCN method by making several assumptions: (a) the x-ray attenuation by the signal is much smaller than that by the background tissue, (b) the quantum noise variance is constant over the field of view of the detector for a given projection angle, and (c) the detector blur is spatially invariant. The formulation of the reconstruction problem shown in (1) is based on assumption (a). Assumptions (b) and (c) make the inversion of $\mathbf{B}_i \mathbf{K}_i^q \mathbf{B}_i' + \mathbf{K}_i^r$ in (1) easily implementable in the frequency domain with a fast Fourier transform (FFT).

The purpose of the regularization term $R(\mathbf{f})$ is to control the noise level. To formulate the regularizer, we used the hyperbola potential function $\eta(t) = \delta^2(\sqrt{1 + (t/\delta)^2} - 1)$, which is edge preserving. Unlike the spatially weighted non-convex regularization [9] that we proposed to enhance MCs, the regularization used in this work is less aggressive because strong regularization may introduce artifacts to the reconstructed images. Furthermore, the hyperbola is convex and ensures that (1) has a unique minimizer. The regularization was applied to the horizontal and the vertical directions in our previous implementation. Specifically, the regularization $R(\mathbf{f})$ has the following form:

$$R_{4\text{NP}}(\mathbf{f}) = \beta \sum_j \eta([\mathbf{C}_x \mathbf{f}]) + \beta \sum_j \eta([\mathbf{C}_y \mathbf{f}]), \tag{2}$$

where $\mathbf{C}_x$ and $\mathbf{C}_y$ compute finite differences along the horizontal and the vertical directions. The subscript '4NP' represents '4 neighboring pixels'.

The disadvantage of $R_{4\text{NP}}(\mathbf{f})$ is that it encourages sharp edges along the horizontal and the vertical directions, such that a small reconstructed object such as a MC may have the shape of a square, and creating subtle square patterns in the soft tissue structures. In this work, we improved the regularization by implementing the regularization using all 8 neighboring pixels (8NP):

$$R_{8\text{NP}}(\mathbf{f}) = \frac{1}{2}\left(\beta \sum_j \eta([\mathbf{C}_x \mathbf{f}]) + \beta \sum_j \eta([\mathbf{C}_y \mathbf{f}]) + \beta \sum_j \eta([\mathbf{C}_{x-y} \mathbf{f}]) + \beta \sum_j \eta([\mathbf{C}_{x+y} \mathbf{f}])\right), \tag{3}$$

where $\mathbf{C}_{x-y}$ and $\mathbf{C}_{x+y}$ compute finite differences along the two diagonal directions. The factor of 1/2 is included to keep the overall regularization effect at a similar level when comparing with the 4NP regularization.

2.2 Reconstruction without Detector Blur or Noise Correlation

In addition to comparing the 4NP and 8NP regularization, we also investigated the role of each model component in the SQS-DBCN method. The SQS-DBCN method includes the detector blur, the corresponding noise correlation and the regularization. To examine the effects of the detector blur and the noise correlation, we studied the following two reconstruction algorithms:

$$\hat{\mathbf{f}}_{\text{No Detector Blur}} = \text{argmin}_{\mathbf{f}} \frac{1}{2} \sum_i \|\mathbf{y}_i - \mathbf{A}_i \mathbf{f}\|^2_{(\mathbf{K}_i^q + \mathbf{K}_i^r)^{-1}} + R(\mathbf{f}), \tag{4}$$

$$\hat{\mathbf{f}}_{\text{No Noise Correlation}} = \text{argmin}_{\mathbf{f}} \frac{1}{2} \sum_i \|\mathbf{y}_i - \mathbf{B}_i \mathbf{A}_i \mathbf{f}\|^2_{(\mathbf{K}_i^q + \mathbf{K}_i^r)^{-1}} + R(\mathbf{f}), \quad (5)$$

The no-detector-blur (noDB) reconstruction neglects the detector blur by setting the point spread function to a Kronecker impulse such that $\mathbf{B}_i$ becomes an identity matrix. This is equivalent to a common approach to SQS regularized reconstruction that ignores detector blur and noise correlation. For the no-noise-correlation (noNC) reconstruction, we keep the detector blur in the system model while neglecting the noise correlation caused by the detector blur so that the effect of the correlated noise model in SQS-DBCN can be evaluated. Another case is that we keep both the detector blur and noise correlation while neglecting the regularization.

2.3 Performance Evaluation and Figures of Merit

The regularization and reconstruction methods were applied to DBT of both breast phantom and human subjects. The phantom consisted of a stack of five 1-cm-thick 50% adipose/50% glandular heterogeneous slabs that simulated the composition and parenchymal pattern of the breast [4]. Clusters of calcium carbonate specks of three nominal size ranges (0.25-0.30mm, 0.18-0.25mm, and 0.15-0.18mm) simulated MCs of different conspicuity levels. Several clusters of each size group were sandwiched at random locations between the slabs. The DBT system acquired 21 projections in 3^o increments over a 60^o arc using a flat panel CsI/a:Si detector with a pixel pitch of 0.1 mm x 0.1 mm. All DBTs were reconstructed at 0.1 mm x 0.1 mm pixel size and 1 mm slice spacing. To simulate the DBT acquired with a GE commercial system, we used the 9 central projections for reconstruction, corresponding to DBT of 24^o scan angle. Two DBT scans with invasive ductal carcinomas in human subjects acquired with IRB approval were also included to evaluate the visual quality of mass margins and soft tissue structures.

The quality of DBT reconstructed with 4NP and the 8NP regularization were visually compared. The difference map was calculated between the two types of the regularization. To compare SQS-DBCN with the noDB and the noNC reconstructions, we used the CNR of MCs as a figure-of-merit. The contrast of an MC was obtained from the peak value of a 2D Gaussian fitted to the MC. The root-mean-square noise was estimated from a noise patch near each cluster of MCs. The mean and standard deviation of the CNR for a given reconstruction condition were estimated from over 30 MCs for each size group. The simultaneous algebraic reconstruction technique with multiscale bilateral filtering (SART-MSBF) method [10] that our lab previously developed was used as a baseline for comparison.

3. RESULTS

Figure 1 and Figure 2 show the difference between the 4NP regularization and the 8NP regularization for an MC cluster in the phantom and a mass in human subject DBT, respectively. With the 4NP regularization, the background texture looks like a lot of overlapping squares, which is caused by the 4NP regularization that encourages sharp edge along the horizontal and the vertical directions. With the 8NP regularization, the background texture looks more smooth and natural. The difference map between the 4NP and the 8NP shows clearly that the "square" texture is reduced with the 8NP regularization.

Figure 3 shows the CNR curves as a function of β with the SQS-DBCN reconstruction, the noDB reconstruction and the noNC reconstruction. We also plotted the CNR level of the SART-MSBF method as a reference. For both the small-sized (0.15-0.18mm) and the medium-sized (0.18-0.25mm) MCs, the SQS-DBCN method achieved a much higher CNR compared with the methods that excluded one of the model components. The SQS-DBCN method also provided a wider range of β values such that the new method will generate higher CNR values compared with SART-MSBF. The large-sized MCs have a similar trend but the CNR curves are not shown here. The reconstruction that included both the detector blur and noise correlation while neglecting the regularization resulted in extremely noisy images after only 2 to 3 SQS iterations so that we omit these results.

Figure 4 shows one MC cluster from each size group reconstructed with the four methods. Note that the β value used here ($\beta = 80$) was not the value corresponding to the highest CNR (Figure 3). The β value that gave the highest CNR over-enhanced the high-frequency texture in the background. The preferred β values for each method were chosen such that both the MCs and the soft tissue structures and mass margins are acceptable. Figure 4 shows that the noDB method generated bumpy texture in the background, while the noNC images were generally more blurred. On the other hand, the image patches with the SQS-DBCN method have sharp MCs while preserving the texture. Figure 5 shows a part of a large spiculated mass in a DBT slice reconstructed with the different methods. Similar to the phantom, the reconstructed images when either the detector blur or the noise correlation is ignored have bumpy background. The SQS-DBCN method gives the best reconstruction results in general. This study demonstrated that both the detector blur and the noise correlation models are important components in the SQS-DBCN method.

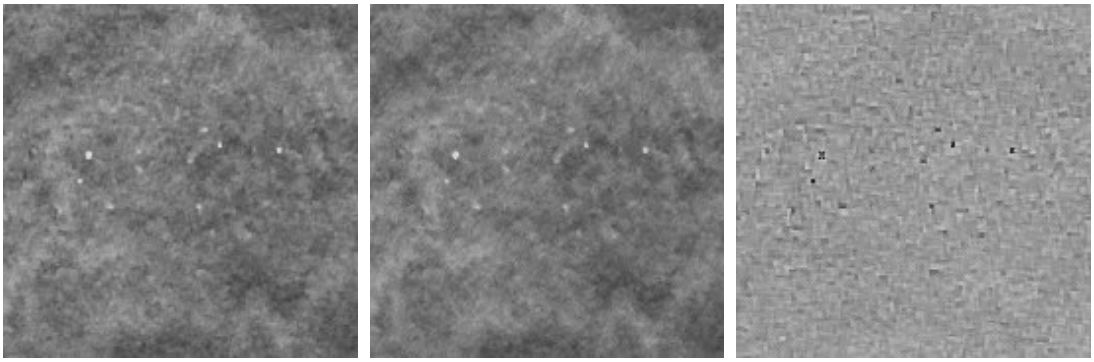

(a) 4NP Regularization (b) 8NP Regularization (c) Difference (8NP - 4NP)

Figure 1. A reconstructed MC cluster from the breast phantom with (a) 4NP, (b) 8NP regularizations, and (c) their difference. The parameters used in the SQS-DBCN method are $\delta = 0.002/mm$, $\beta = 80$. The 8NP regularization provides more natural-looking texture. The contrast of MCs with the 8NP method is slightly lower than those with the 4NP but the 8NP image has higher CNR because of a lower noise level. The size of the image patches is 180×180 (1 pixel = 0.1 mm x 0.1 mm).

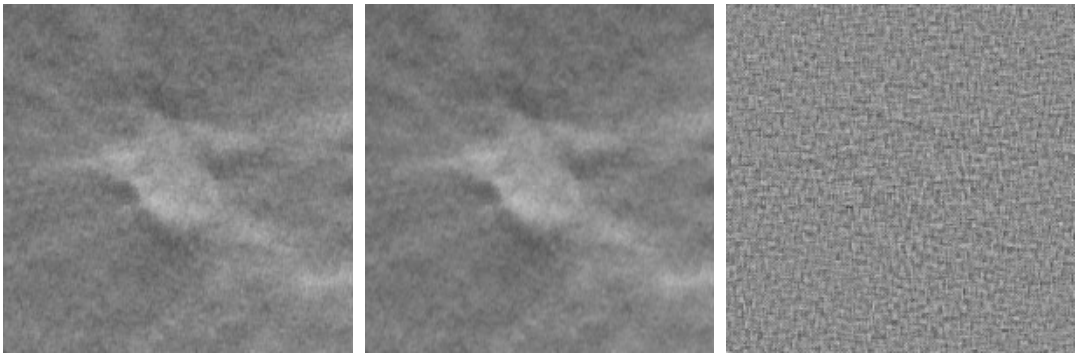

(a) 4NP Regularization (b) 8NP Regularization (c) Difference (8NP - 4NP)

Figure 2. A 5-mm invasive ductal carcinoma in a human subject DBT slice reconstructed with (a) 4NP, (b) 8NP regularizations and (c) their difference. The parameters in the SQS-DBCN were $\delta = 0.002/mm$, $\beta = 80$. The 8NP method reduces artifacts in the texture. The size of the image patches is 200×200 (1 pixel = 0.1 mm x 0.1 mm).

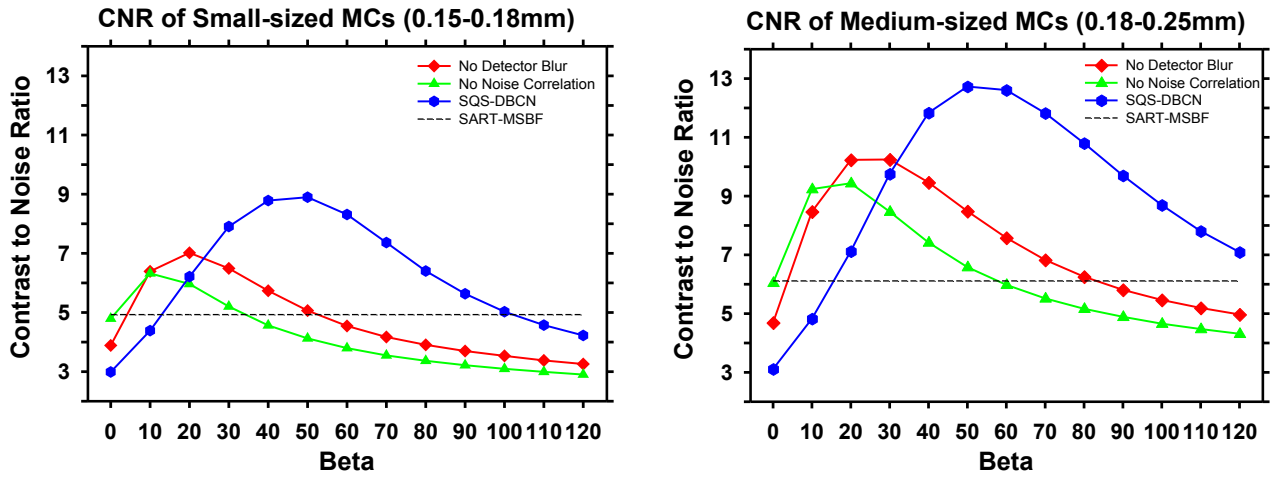

Figure 3. CNR of MCs of two different sizes as a function of the regularization parameter β when δ is fixed at 0.002/mm. The SQS-DBCN method is able to reconstruct MCs with higher CNR compared with the no-detector-blur or the no-noise-correlation reconstructions.

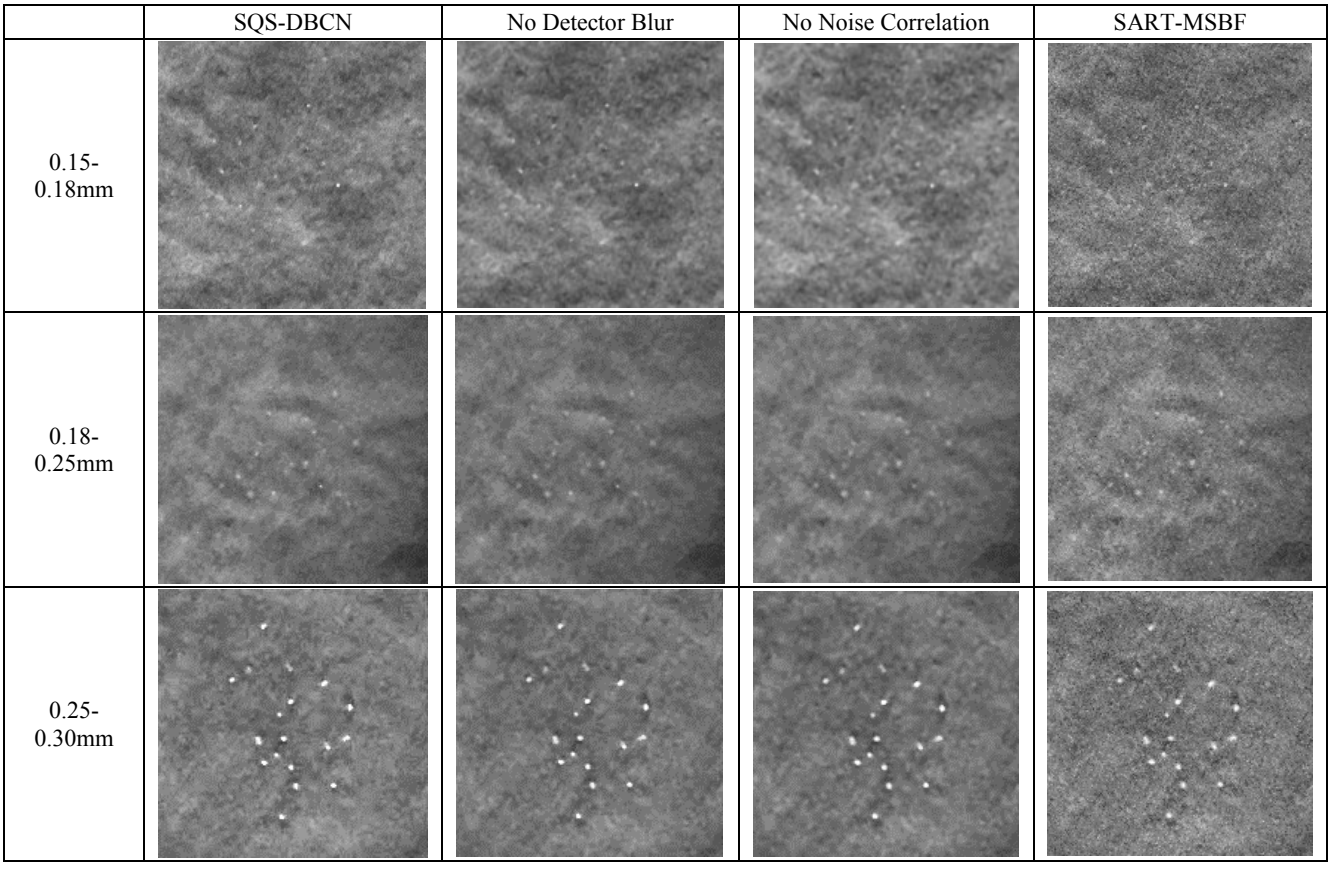

Figure 4. MC clusters of different sizes in the breast phantom DBT reconstructed with four different methods ($\delta = 0.002/\text{mm}$, $\beta = 80$). All ROIs are 180 x 180 pixels in size (1 pixel = 0.1 mm x 0.1 mm).

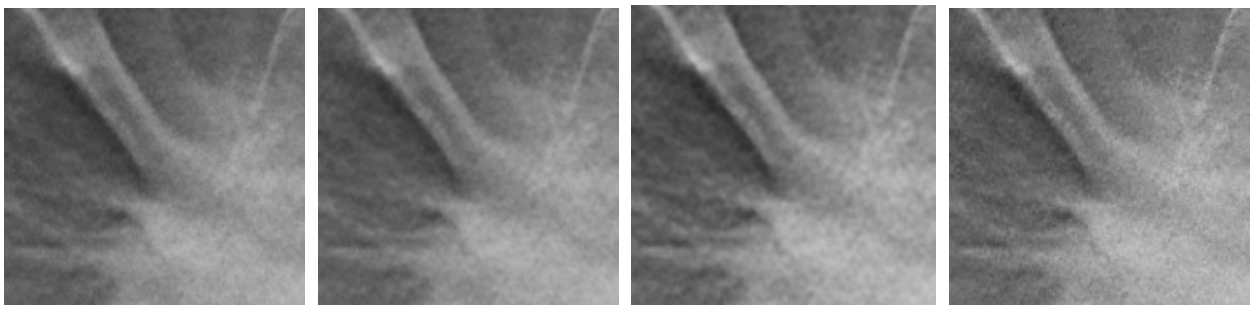

(a) SQS-DBCN (b) No Detector Blur (c) No Noise Correlation (d) SART-MSBF

Figure 5. Comparison of the four methods for the DBT of an invasive ductal carcinoma in a breast with spiculations ($\delta = 0.002/\text{mm}, \beta = 80$). Only a small part of the mass is shown to have a close-up view the spiculations.

Our results showed that regularizing with diagonal directions reduced artifacts and the noise level. It effectively eliminated the square texture resulting from enhancing sharp edges along the horizontal and vertical directions in the previous implementation. The SQS-DBCN reconstructed images had better image quality than reconstructions without modeling detector blur or correlated noise, as indicated by the CNR of MCs and textural artifacts. These results indicated that regularized DBT reconstruction with detector blur and correlated noise modeling, even with simplifying assumptions, can improve DBT image quality compared to that without system modeling.

4. CONCLUSIONS

In this work, we showed that the 8NP regularization is better than the 4NP regularization in reducing artifacts in the reconstructed DBT images. The SQS-DBCN method that incorporated both the detector blur and correlated noise models is superior to those neglecting one of the model components. However, our current SQS-DBCN method depends on several assumptions and good parameter selection. Further study is needed to develop adaptive methods to select the parameters, better estimation of noise variance, and more general model to relax the assumptions. This study also indicates that a more complete model-based reconstruction may further improve the DBT image quality. We will continue to investigate methods to implement other system model components such as focal spot blur, scatter, and beam hardening.

ACKNOWLEDGEMENTS

This work is supported by National Institutes of Health grant number R01 CA151443.

REFERENCES

[1] B. E. H. Claus, J. W. Eberhard, A. Schmitz *et al.*, "Generalized Filtered Back-Projection Reconstruction in Breast Tomosynthesis," Lecture notes in computer science – digital mammography, 4046, 167-174 (2006).
[2] T. Mertelmeier, J. Orman, W. Haerer *et al.*, "Optimizing filtered backprojection reconstruction for a breast tomosynthesis prototype device," Proc. SPIE, 6142, 61420F (2006).
[3] G. Lauritsch, and W. Haerer, "A theoretical framework for filtered back-projection in tomosynthesis," Proc. SPIE, 3338, 1127-1137 (1998).
[4] Y. Zhang, H.-P. Chan, B. Sahiner *et al.*, "A comparative study of limited-angle cone-beam reconstruction methods for breast tomosynthesis," Medical Physics, 33(10), 3781-3795 (2006).

[5] J. G. Bian, K. Yang, J. M. Boone *et al.*, "Investigation of iterative image reconstruction in low-dose breast CT," Physics in Medicine and Biology, 59(11), 2659-2685 (2014).
[6] E. Y. Sidky, X. Pan, I. Reiser *et al.*, "Enhanced imaging of microcalcifications in digital breast tomosynthesis through improved image-reconstruction algorithms," Medical Physics, 36(11), 4920-4932 (2009).
[7] J. Zheng, J. A. Fessler, and H.-P. Chan, "Digital Breast Tomosynthesis Reconstruction with Detector Blur and Correlated Noise," Proc. 4th International Conference on Image Formation in X-Ray Computed Tomography, CT-Meeting 2016, 21-24 (2016).
[8] J. Zheng, J. A. Fessler, and H.-P. Chan, "Segmented Separable Footprint Projector for Digital Breast Tomosynthesis and Its application for Subpixel Reconstruction," Medical Physics, 44, (in press) (2017).
[9] J. Zheng, J. A. Fessler, and H.-P. Chan, "Digital Breast Tomosynthesis Reconstruction using Spatially Weighted Non-convex Regularization," Proc. SPIE, 9783, 978369 (2016).
[10] Y. Lu, H. P. Chan, J. Wei *et al.*, "Multiscale Regularized Reconstruction for Enhancing Microcalcification in Digital Breast Tomosynthesis," Proc SPIE, 8313, 831322 (2012).